Hybrid numerical modeling of a 50 W-Class Annular Hall Thruster

Arturo Popoli, Andrea Cristofolini, Laurent Garrigues, Dongho Lee, Guentae Doh, Holak Kim, Wonho Choe

Hybrid numerical modeling of a 50 W-Class Annular Hall Thruster

IEPC-2022-364

Presented at the 37th International Electric Propulsion Conference
Massachusetts Institute of Technology, Cambridge, MA, USA
June 19-23, 2022

Arturo Popoli[1] and Andrea Cristofolini[2]
University of Bologna, Viale Risorgimento 2, 40136 Bologna, Italy

Laurent Garrigues[3]
LAPLACE, Université de Toulouse, CNRS, 118 route de Narbonne, 31062 Toulouse, Cedex 9, France

Dongho Lee[4], Guentae Doh[5] Holak Kim[6] and Wonho Choe[7]
Korea Advanced Institute of Science and Technology (KAIST), Daejeon 34141, Republic of Korea

In this work we perform a computational study on a 50 W-class miniaturized annular Hall thruster for space propulsion. The employed code is based on a 2D axisymmetric hybrid formulation, where ions and electrons are described using a kinetic and a fluid approach, respectively. The cross-field anomalous electron transport is modeled empirically, by enforcing a continuous collision frequency profile both inside the thruster channel and in the near-field plume. The simulation results are compared to experimental measurements on the laboratory thruster, to both assess the influence of anomalous transport for the considered thruster and predict the measured global performance.

I. Nomenclature

n, n_0	=	plasma number density and reference plasma number density
Ω_{iz}	=	ionization rate
$\mathbf{\Gamma_e}$, $\mathbf{\Gamma_i}$, $\Gamma_{e,\perp}$	=	electron and ion flux, cross-field electron flux
$\Gamma_{i,W}$, $\Gamma_{i,W}$	=	ion and electron fluxes directed toward walls
$\mu_\perp$	=	total cross-field electron mobility
μ_C	=	electron mobility due to Coulomb collisions
$\mu_{\mathrm{e-Xe}}$	=	electron mobility due to collisions with neutrals
μ_{an}	=	anomalous electron mobility
$\mathbf{E}$, $E_\perp$	=	electric field and electric field component perpendicular to the magnetic field
T_e, ϵ	=	electron temperature and electron mean energy
e	=	elementary charge
φ	=	electric potential
λ	=	magnetic stream function used to construct the fluid grid
B_z, B_r	=	axial and radial magnetic field components

[1]Postdoctoral researcher, Dipartimento di Ingegneria Elettrica, Elettronica e dell'Informazione "Guglielmo Marconi", arturo.popoli@unibo.it.
[2]Associate professor, Dipartimento di Ingegneria Elettrica, Elettronica e dell'Informazione "Guglielmo Marconi", andrea.cristofolini@unibo.it.
[3]Director of Research, CNRS, LAPLACE, laurent.garrigues@laplace.univ-tlse.fr.
[4]Graduate student, Department of Physics; dhlee.phys@kaist.ac.kr
[5]Graduate student, Department of Physics; guentaedoh@kaist.ac.kr
[6]Postdoctoral researcher, Department of Physics; holakkim@kari.re.kr
[7]Professor, Department of Nuclear and Quantum Engineering; wchoe@kaist.ac.kr

$\mathbf{q_e}$ = conduction heat flux
$C_{e,in}$ = electron energy density source term due to inelastic collisions with other species
W = effective loss coefficient for collisions between electrons and walls

II. Introduction

In recent years considerable interest has grown towards micro and nano-satellites for various military and civil missions. The latter category includes telecommunications, Earth observation and a broad range of scientific missions [1]. This has in turn let to a corresponding technical need for compact low power and low thrust plasma propulsion devices for orbit transfers, station-keeping and attitude control [2].

In this context, numerical models capable of accurately reproducing the performance and the main physical phenomena of thrusters are an important tool not only from the perspective of reducing the high costs associated with prototyping and testing, but also for gaining further insight into the basic physics of these devices.

In this work a hybrid numerical model is used to assess the performance and the acceleration structure of a miniaturized low-power annular Hall thruster (AHT) developed at KAIST [3]. The employed numerical model is briefly described in Section III, while the obtained results are discussed and compared to experimental measurements in Section IV.

III. Model Description

The employed model shares many features with the 2D models previously developed by Fife [4] and Komurasaki and colleagues [5]. The main strategy is based on using two different numerical approaches to study the dynamics of electrons and heavy (neutral and ion) species.

The heavies are described with a particle approach on a 2D $r-z$ axisymmetric Cartesian grid, such as the one shown in Fig. 1. Note that in reality the grid spacing is non-uniform and a finer spatial discretization is employed within the thruster channel, where larger plasma densities are expected. Neutral particles (Xe) are injected from the anode with a Maxwellian velocity distribution and followed up to the domain boundary downstream of the channel exit. Single (Xe^+) and double (Xe^{++}) ions are also considered as macro-particles, accelerated by the electric field. These are generated by inelastic collisions between electrons and neutrals and lost at walls due to recombination.

Regarding electrons, these are instead modeled with a fluid approach, based on solving the first three moments of the Boltzmann equation. The number density conservation equation is expressed as:

$$-\frac{\partial n}{\partial t} + \Omega_{iz} = \boldsymbol{\nabla} \cdot \boldsymbol{\Gamma}_\mathbf{e} = \boldsymbol{\nabla} \cdot \boldsymbol{\Gamma}_\mathbf{i}, \tag{1}$$

where the electron flux is equal to the ion flux for the quasi-neutrality assumption. Note that the latter is obtained at each time-step from the particle model of the ion species.

Since the electrons are strongly magnetized by the static magnetic field, the two components of $\boldsymbol{\Gamma}_\mathbf{e}$ in Eq. 1 (parallel and perpendicular to the generic magnetic field line) can be considered separately.

The perpendicular component, i.e., the cross-field electron flux, is assumed to be due to the combination of a drift and a diffusion term:

$$\Gamma_{e,\perp} = -\mu_\perp E_\perp n - \frac{2}{3e}\mu_\perp \boldsymbol{\nabla}_\perp (n\epsilon), \tag{2}$$

where the electron mobility is given by:

$$\mu_\perp = \mu_C + \mu_{\mathrm{e-Xe}} + \mu_{an}. \tag{3}$$

The cross-field mobility in Eq. 3 is expressed as the sum of two *classic* terms (μ_C, $\mu_{\mathrm{e-Xe}}$) due to collisions with other particles and an anomalous contribution (μ_{an}). The latter summarizes the effects of electron-wall interactions (near-wall conductivity) inside the channel as well as turbulence and instabilities in the near-field plume.

Finally, the electron mean energy density balance is:

$$\frac{\partial (n\epsilon)}{\partial t} + \frac{5}{3}\boldsymbol{\nabla} \cdot (\boldsymbol{\Gamma}_\mathbf{e}\epsilon) + \boldsymbol{\nabla} \cdot \mathbf{q_e} = -e\mathbf{E} \cdot \boldsymbol{\Gamma}_\mathbf{e} - C_{e,in} - nW, \tag{4}$$

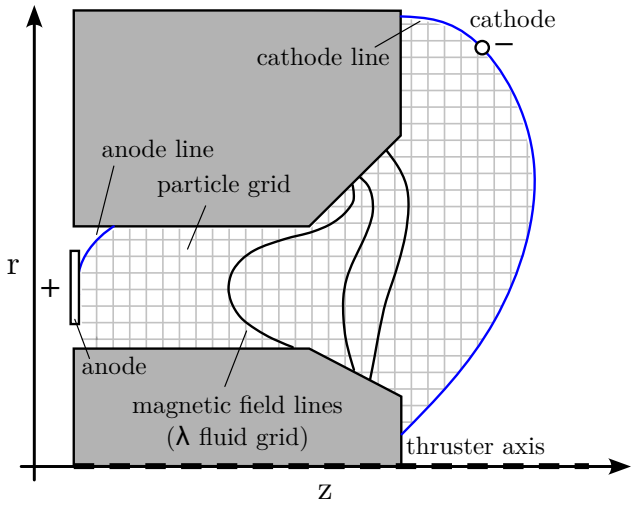

Fig. 1 Sketch of the calculation domain, with the 2D $r-z$ grid employed for the heavy species and the fluid quasi-1D for the electrons; neutrals are injected in the domain from the anode; the domain is limited by the two magnetic field lines intersecting the anode and the cathode.

where $\mathbf{E}\cdot\mathbf{\Gamma_e}$ represents electron heating due to the electric field. The term $C_{e,in}$ summarizes the energy losses due to inelastic collisions with other particles, i.e., electronic excitation and ionization. The considered processes and their respective rate coefficients are reported in [6]. Finally, nW represents energy losses due to wall interactions.

For a Maxwellian energy distribution function, the effective energy loss per unit time coefficient can be obtained from the balance between electron energy flux to and from a generic wall element [7]. The electron energy flux can be related to the ion flux, giving:

$$W = \frac{\iint_S \Gamma_{i,W}\,\mathrm{d}S}{\iiint_V n\,\mathrm{d}V}\left[\frac{4(\epsilon-\bar{\gamma}\epsilon_s)}{3(1-\bar{\gamma})}+\varphi_s\right], \tag{5}$$

where $\iint_S \Gamma_{i,W}$ is the number of ions colliding with a wall element between two consecutive magnetic field lines per unit time, and $\iiint_V n\,dV$ is the number of ions (and electrons) in the volume between the two considered lines; $\bar{\gamma}$ is the secondary electron emission (SEE) yield, integrated over a Maxwellian distribution, and ϵ_s is the electron mean energy of wall-emitted electrons [8]; φ_s is the sheath potential, obtained from the zero-current condition at walls $\Gamma_{i,W}=\Gamma_{e,W}(1-\bar{\gamma})$ and the assumption of a linear dependence of the SEE yield from the electron mean energy [8]:

$$\varphi_s = \frac{2}{3}\epsilon\ln\left[(1-\bar{\gamma})\sqrt{\frac{m_i}{2\pi m_e}}\right], \tag{6}$$

Equations 2 and 4 are solved in the cross-field direction on a quasi-1D grid. The latter, as shown in Fig. 1, is constructed by means of a magnetic stream function λ, defined as $\frac{\partial\lambda}{\partial z}=rB_r$, $\frac{\partial\lambda}{\partial r}=-rB_z$. The function λ is constant along the magnetic field lines ($\mathbf{B}\cdot\boldsymbol{\nabla}\lambda=0$). In this way, the variables in the transport equations are spatially derived with respect to a quantity that is invariant along magnetic field lines [4].

Along the generic line, the drift and diffusion terms in Eq. 2 must be balanced to ensure current conservation. This implies that ϵ is constant along the magnetic field lines, and the electric potential can be obtained from Morozov's relation [9]:

$$\varphi = \varphi^*(\lambda)+\frac{2}{3e}\epsilon(\lambda)\ln\left(\frac{n}{n_0}\right) \tag{7}$$

The numerical discretization of the set of transport equations can be found in [10]. The electron anomalous transport treatment is also described in [11].

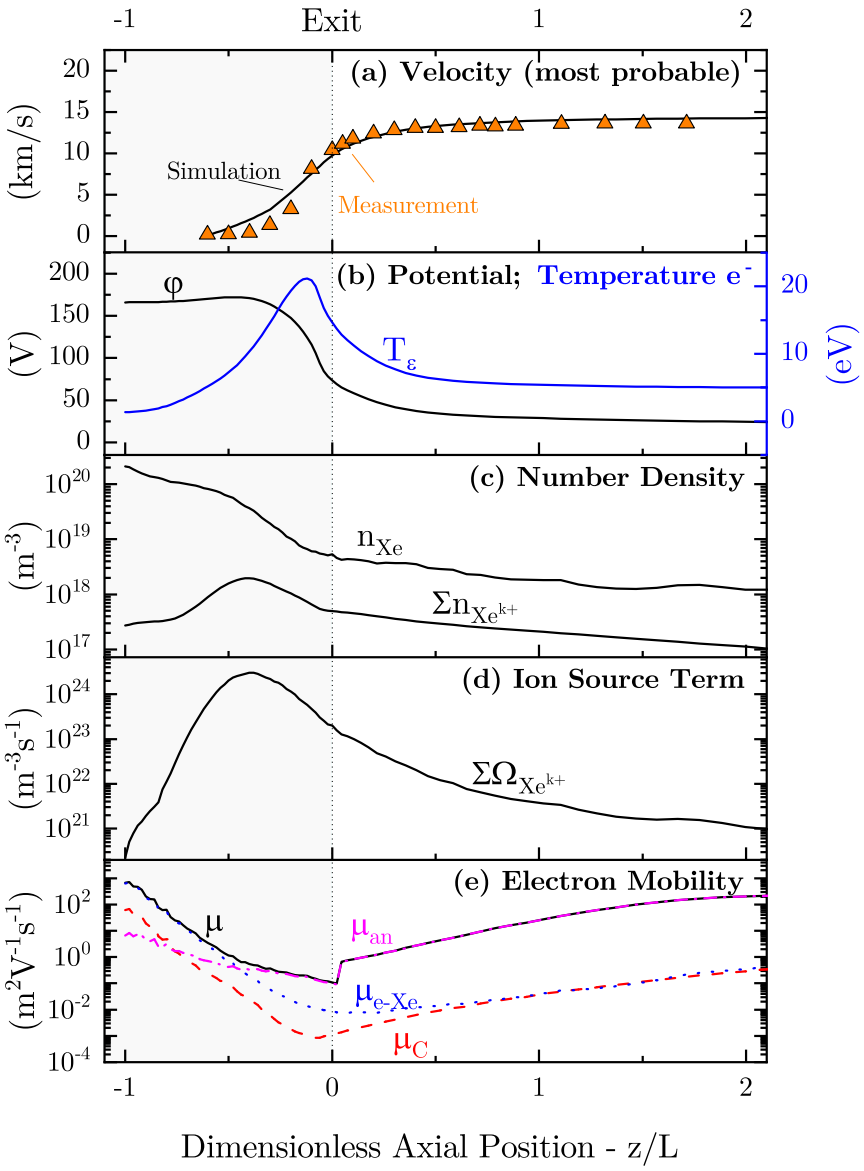

Fig. 2 Simulation results along the mid-channel line.

IV. Simulation Results

We simulate the considered 50 W-class miniaturized thruster assuming a flow rate $\dot{m} = 0.42\,\mathrm{mg\,s^{-1}}$ and an anode voltage $V_a = 200\,\mathrm{V}$. As described in [12], these operational conditions correspond to *mode B* (as opposed to *mode A*, found for lower flow rates and anode voltages). The numerical simulations are performed assuming a temperature $T_{\mathrm{Xe}} = 500\,\mathrm{K}$ for the neutrals, and a background pressure $p_{bg} = 1\,\mathrm{mPa}$. For what concerns the electron energy conservation equation, the two boundary conditions $T_{e,\mathrm{anode}} = 1.3\,\mathrm{eV}$ and $T_{e,\mathrm{cathode}} = 5\,\mathrm{eV}$ are enforced along the anode and cathode magnetic lines, respectively. The anomalous electron mobility μ_{an} is iteratively adjusted to match the experimentally measured most-probable ion velocity along the mid-channel line and discharge current.

The spatial evolution along the mid-channel line of several physical quantities are shown in Fig. 2. First, the simulated (most probable) ion velocity is compared to the laser-induced fluorescence (LIF) experimental measurements in Fig. 2(a). The main acceleration of the ions takes place near the channel exit, where one can also find the maximum electron temperature in Fig. 2(b). As one can notice, the electric potential enforced at the anode (as a Dirichlet boundary condition) is lower than 200 V. This choice is made to account for the experimentally measured electrostatic potential in the near-field plume reducing the accelerating voltage drop between the two electrodes. This behavior is likely linked to the hollow cathode operation. From 2(c) one can notice that – in contrast to full-scale thrusters – there is a considerable availability of neutrals (n_{Xe}) downstream of the ionization region. The line marked as $\sum n_{\mathrm{Xe}^{k+}}$ indicates the sum of singly and doubly charged ion number density. Note that the peak value is located slightly upstream of the peak T_ϵ. The same feature characterizes the ion source term sum $\sum \Omega_{\mathrm{Xe}^{k+}}$ in Fig. 2(d). The single ions are produced by ionization from ground state neutrals ($\mathrm{Xe} \longrightarrow \mathrm{Xe}^{+}$). Double ions are obtained from step-wise ionization from single ions ($\mathrm{Xe}^{+} \longrightarrow \mathrm{Xe}^{++}$) and double ionization from neutrals ($\mathrm{Xe} \longrightarrow \mathrm{Xe}^{++}$). Finally, the electron mobility terms of Eq. 3 are plotted in Fig. 2(e). As one can see, the total electron mobility (μ) near the anode is mainly due to collisions between electrons and neutrals, thanks to the large availability of Xe. Indeed, When n_{Xe} decreases in the vicinity of the channel exit, the anomalous mobility term becomes dominant. Note that a sharp mobility change is needed downstream of the channel exit to localize the voltage drop (end the electric field peak value) inside the discharge channel. Conversely, the contribution of Coulomb collisions between electrons and ions is limited throughout the whole computational domain.

The computed global performance, corresponding to the results shown in Fig. 2, is summarized in Table 1. The computed values – obtained by enforcing the continuous electron mobility profile in Fig. 2(e) – are in good agreement with the measurements. The computed doubly-charged ion current fraction $I(\mathrm{Xe}^{++})/I(\mathrm{Xe}^{+})$ is also in agreement with the measured value, showing that a significant generation of double ions is achieved for the considered thruster.

Table 1 Measured and simulated global thruster performance. Results marked with * are corrected to account for the reduced applied voltage.

Parameter	Simulated	Measured
Thrust	3.80 mN	3.78 mN*
Anode efficiency	0.28	0.28*
Discharge current	0.31 A	0.30 A
$I(\mathrm{Xe}^{++})/I(\mathrm{Xe}^{+})$	9.96 %	10 %

V. Conclusions

A miniaturized annular Hall thruster was simulated with a hybrid 2D $r-z$ kinetic-fluid code based featuring an empirical numerical treatment of the anomalous electron transport.

The cross-field mobility iterative adjustment based on the LIF-measured ion velocity profile allowed to achieve a good agreement between the simulated and measured global performance, doubly-charged ions generation and overall acceleration structure of the thruster.

The performed study also highlights that – at least for the particular thruster under consideration – adequate modeling of the hollow cathode effects on the local electric potential is essential to reproduce the main physical features of the device.

Acknowledgments

The authors thank the Partnership Hubert Curien (PHC) Star Program between France and Republic of Korea and the Science and Technology Amicable Relationships (STAR) Program (NRF-2019K1A3A1A21031236).

References

[1] Mazouffre, S., and Grimaud, L., "Characteristics and Performances of a 100-W Hall Thruster for Microspacecraft," *IEEE Transactions on Plasma Science*, Vol. 46, No. 2, 2018, pp. 330–337. https://doi.org/10.1109/TPS.2017.2786402.

[2] Keidar, M., Zhuang, T., Shashurin, A., Teel, G., Chiu, D., Lukas, J., Haque, S., and Brieda, L., "Electric propulsion for small satellites," *Plasma Physics and Controlled Fusion*, Vol. 57, No. 1, 2014, p. 014005. https://doi.org/10.1088/0741-3335/57/1/014005.

[3] Lee, D., Kim, H., Lee, S., Doh, G., and Choe, W., "Development and performance test of a 50 W-class Hall thruster," *36th International Electric Propulsion Conference (Vienna, Austria)*, 2019.

[4] Fife, J. M., "Hybrid-PIC modeling and electrostatic probe survey of Hall thrusters," PhD Thesis, Massachusetts Institute of Technology, 1998.

[5] Komurasaki, K., and Arakawa, Y., "Two-dimensional numerical model of plasma flow in a Hall thruster," *Journal of Propulsion and Power*, Vol. 11, No. 6, 1995, pp. 1317–1323. https://doi.org/10.2514/3.23974.

[6] Garrigues, L., "Ion properties in a Hall current thruster operating at high voltage," *Journal of Applied Physics*, Vol. 119, No. 16, 2016, p. 163305. https://doi.org/10.1063/1.4947523.

[7] Garrigues, L., Hagelaar, G. J. M., Boniface, C., and Boeuf, J. P., "Anomalous conductivity and secondary electron emission in Hall effect thrusters," *Journal of Applied Physics*, Vol. 100, No. 12, 2006, p. 123301. https://doi.org/10.1063/1.2401773.

[8] Barral, S., Makowski, K., Peradzyński, Z., Gascon, N., and Dudeck, M., "Wall material effects in stationary plasma thrusters. II. Near-wall and in-wall conductivity," *Physics of Plasmas*, Vol. 10, No. 10, 2003, pp. 4137–4152. https://doi.org/10.1063/1.1611881.

[9] Morozov, A. I., and Savel'ev, V. V., "One-Dimensional hybrid model of a stationary plasma thruster," *Plasma Physics Reports*, Vol. 26, No. 10, 2000, pp. 875–880. https://doi.org/10.1134/1.1316827.

[10] Hagelaar, G. J. M., Bareilles, J., Garrigues, L., and Boeuf, J. P., "Two-dimensional model of a stationary plasma thruster," *Journal of Applied Physics*, Vol. 91, No. 9, 2002, pp. 5592–5598. https://doi.org/10.1063/1.1465125.

[11] Hagelaar, G. J. M., Bareilles, J., Garrigues, L., and Boeuf, J. P., "Role of anomalous electron transport in a stationary plasma thruster simulation," *Journal of Applied Physics*, Vol. 93, No. 1, 2002, pp. 67–75. https://doi.org/10.1063/1.1527218.

[12] Lee, D., Doh, G., Kim, H., Garrigues, L., and Choe, W., "Distinct discharge modes in micro Hall thruster plasmas," *Plasma Sources Science and Technology*, Vol. 30, No. 3, 2020, p. 035004. https://doi.org/10.1088/1361-6595/abdf19.